World Journal of Pharmaceutical and Life Sciences

www.wjpls.org

Impact Factor: 8.21 Coden USA: WJPLA7

IN SILICO CONSTRUCTION AND MOLECULAR-DYNAMICS VALIDATION OF A TRIPLE-MUTANT (K103N/Y181C/Y188L) HIV-1 REVERSE TRANSCRIPTASE AND STRUCTURE-BASED SCREENING OF THYMOQUINONE-DERIVED NON-NUCLEOSIDE INHIBITORS

Chandewar A. V.[a], Devani A.[b], Kamil R. F.[a]*

[a]Department of Pharmaceutical Chemistry, Pataldhamal Wadhwani College of Pharmacy, Yavatmal, Maharashtra, India.

***Corresponding Author: Kamil R. F.**

Department of Pharmaceutical Chemistry, Pataldhamal Wadhwani College of Pharmacy, Yavatmal, Maharashtra, India. **DOI:** https://doi.org/10.5281/zenodo.22159616

How to cite this Article: Chandewar A. V., Devani A., Kamil R. F.*. (2026). In Silico Construction and Molecular-Dynamics Validation of A Triple-Mutant (K103n/Y181c/Y188l) Hiv-1 Reverse Transcriptase and Structure-Based Screening of Thymoquinone-Derived Non-Nucleoside Inhibitors. World Journal of Pharmaceutical and Life Sciences, 12(9), 54–61.

Article Received on 15/07/2026 **Article Revised on 04/08/2026** **Article Published on 01/09/2026**

ABSTRACT

Resistance mutations in the non-nucleoside inhibitor binding pocket (NNIBP) of HIV-1 reverse transcriptase (RT) — most prominently K103N, Y181C and Y188L — continue to erode the durability of the entire non-nucleoside reverse transcriptase inhibitor (NNRTI) class. We report an integrated computational workflow that (i) builds and validates a single, clinically representative RT model carrying all three mutations simultaneously, and (ii) uses that model to prioritise novel chemotypes seeded from the natural-product quinone thymoquinone (TQ). The p66 catalytic subunit of wild-type RT (PDB 2BAN) was edited to introduce K103N, Y181C and Y188L, and the triple mutant (designated 2BAP) was generated by comparative modelling in MODELLER using the single-mutant crystal structures 3MED, 1JKH and 2YNF as templates. The model was energy-minimised and relaxed by a 100 ns explicit-solvent molecular-dynamics (MD) simulation in NAMD. Stereochemical quality improved markedly relative to the parent structure (PROCHECK core-region occupancy 75.2% → 96.0%; ERRAT overall quality factor 65.25 → 78.86, rising to 87.36 after MD), and the backbone RMSD plateaued near 100 ns, indicating a stable, well-packed model. A predefined 24–26 residue NNIBP grid was used for AutoDock-based docking of TQ and of three leads — a virtual-screening-derived pentacenedione (Ligand 1), a rationally assembled pyridin-2(1H)-one (Ligand 2, TQ-PZP-03) and a 3D-QSAR-benchmark pyridinone (Ligand 3, VC1) — against wild-type and the K103N, Y181C, Y188L and triple-mutant structures. All leads occupied the NNIBP and, critically, retained their binding scores across the mutant panel rather than collapsing at Y181C/Y188L. In-silico ADMET (SwissADME) and toxicity (ProTox) profiling passed the leads through standard drug-likeness filters, while an efavirenz benchmark exposed the limited applicability domain of the toxicity model for this chemical space. The validated triple-mutant model and the retained cross-mutant docking profiles together provide a structure-based rationale for advancing the pyridinone leads to experimental evaluation.

KEYWORDS: HIV-1 reverse transcriptase; NNRTI resistance; Homology modelling; Molecular dynamics; Molecular docking; Thymoquinone; Virtual screening.

1. INTRODUCTION

Human immunodeficiency virus type 1 (HIV-1) reverse transcriptase (RT) is a validated and heavily exploited antiretroviral target because it performs an obligatory, virus-specific step of the replication cycle: the conversion of the single-stranded RNA genome into double-stranded proviral DNA. The enzyme is an asymmetric heterodimer of a 66 kDa (p66) and a 51 kDa (p51) subunit; the polymerase active site and the adjacent allosteric non-nucleoside inhibitor binding pocket (NNIBP) both reside in p66. Non-nucleoside reverse transcriptase inhibitors (NNRTIs) bind the NNIBP roughly 10 Å from the catalytic aspartates and act as non-competitive, allosteric brakes on polymerisation,

distorting the geometry of the active site rather than competing with substrate.

Despite their central role in first-line therapy, the NNRTI class remains structurally fragile in the face of resistance. A small number of NNIBP substitutions — notably K103N, Y181C and Y188L — recur across global surveillance datasets and confer broad cross-resistance that spans first-, second- and, increasingly, third-generation agents. Because these substitutions accumulate under drug pressure and are transmitted, an inhibitor that retains potency only against wild-type enzyme has limited translational value. The design problem is therefore not simply to find a molecule that binds the wild-type NNIBP, but to find one whose binding is robust to the simultaneous presence of the principal resistance mutations.

Most reported structure-based studies evaluate candidate inhibitors against single-mutant structures considered one at a time, which does not reproduce the multi-mutant genotypes seen clinically. A model that carries K103N, Y181C and Y188L together offers a more demanding and more realistic in-silico filter. Constructing such a composite structure by comparative modelling — using the individual single-mutant crystal structures as templates — is a tractable route to that goal, provided the resulting model is rigorously validated for stereochemistry and dynamic stability before it is used for docking.

On the ligand side, natural-product quinones offer an underexplored starting point. Thymoquinone (TQ), the principal bioactive constituent of Nigella sativa seed, is a small p-benzoquinone with a wide pharmacological profile but no established anti-HIV pharmacophore and a reactive Michael-acceptor motif that limits its developability. TQ is nonetheless attractive as a seed structure: it is synthetically simple, and its quinone core can be recast into a pyridin-2(1H)-one — the hydrogen-bond-donor scaffold that anchors clinically used pyridinone NNRTIs in the NNIBP. This motivates a scaffold-hopping strategy in which TQ is used to nucleate larger, pocket-filling leads.

Here we report the computational half of an integrated discovery programme. We (i) construct a triple-mutant HIV-1 RT model (K103N/Y181C/Y188L, designated 2BAP), validate it stereochemically and equilibrate it by 100 ns MD; (ii) characterise the binding of TQ across wild-type and mutant RT; (iii) perform structure-based virtual screening to derive pocket-filling leads and evaluate them, alongside a 3D-QSAR-benchmark pyridinone, across the full wild-type-plus-mutant panel; and (iv) profile the leads by in-silico ADMET and toxicity prediction. The complementary experimental work — extraction and authentication of TQ, chemical synthesis of the leads, and the in-vitro RT-inhibition bioassay — is reported separately in the companion paper.

2. MATERIALS AND METHODS

2.1. Sequence retrieval and target preparation

The amino-acid sequence and crystal coordinates of wild-type HIV-1 RT were retrieved from the RCSB Protein Data Bank under accession 2BAN. Because the NNIBP and the polymerase site are located exclusively in the p66 (chain A) subunit, chain B (p51) was removed from 2BAN and from every template structure so that modelling and docking focused on the catalytically and pharmacologically relevant subunit. Three NNIBP resistance mutations were selected for modelling on the basis of their prevalence in the Stanford HIV Drug Resistance Database and their status as class-defining substitutions: K103N, Y181C and Y188L. Single-mutant crystal structures were retrieved as modelling templates — 3MED (K103N), 1JKH (Y181C) and 2YNF (Y188L).

2.2. Homology (comparative) modelling of the triple mutant

The wild-type 2BAN sequence was edited in BioEdit to introduce the three substitutions simultaneously, yielding the target sequence 2BAP (K103N, Y181C, Y188L). The target was aligned to the three single-mutant template sequences using ClustalW2. The resulting multiple alignment was submitted to MODELLER 9.14, which builds all-non-hydrogen-atom models by satisfaction of spatial restraints. The best-scoring model was carried forward and designated 2BAP.

2.3. Energy minimisation and molecular-dynamics simulation

The 2BAP model was first relaxed by energy minimisation under the GROMOS96 43B1 parameter set in Swiss-PDB Viewer. For dynamics, hydrogen atoms were added in the Molecular Operating Environment (MOE) and CHARMM22 parameters were assigned. A protein structure file was generated with the AutoPSF module of VMD; the protein was solvated in an explicit water box and neutralised with NaCl ions using the VMD Solvate and Ionize extensions. Solvent and added hydrogens were minimised for 50 000 steps, after which a 100 ns periodic-boundary MD simulation was run in NAMD2 at a constant 310 K. The equilibrated structure was extracted for stereochemical re-validation and used as the docking receptor.

2.4. Model validation

Stereochemical and packing quality were assessed for the wild-type parent (2BAN), the initial 2BAP model, and the post-MD 2BAP structure using the SAVES suite (PROCHECK for Ramachandran distribution; ERRAT for non-bonded atomic interaction statistics) and the ProSA knowledge-based energy server. Root-mean-square deviation (RMSD) between model and template, superimposition, and visual inspection were performed in MOE, UCSF Chimera, PyMOL and Swiss-PDB Viewer. Backbone RMSD versus simulation time was monitored to confirm convergence.

2.5. Definition of the NNIBP and docking protocol

A consensus NNIBP was defined from a combination of wild-type and mutant crystal structures, yielding a set of 24–26 pocket residues (including the mutated positions 103, 181 and 188) used as a reference binding site. Two complementary docking modes were applied. In blind docking, a large grid spanning the entire receptor surface was used to locate binding without prior site assumptions. In residue-based docking, the grid box (100 × 100 × 100 points, 1.0 Å spacing) was centred so as to enclose all predefined NNIBP residues. Before any candidate was docked, native co-crystallised ligands were re-docked into their parent structures to confirm that the protocol reproduced the experimental pose. Blind and pocket-restricted docking were carried out in AutoDock 4.2; large-scale virtual screening used AutoDock Vina. Receptors and ligands were prepared as PDBQT files (charge assignment in AutoDock Tools; ligand geometries built in MarvinSketch and format-converted with Open Babel).

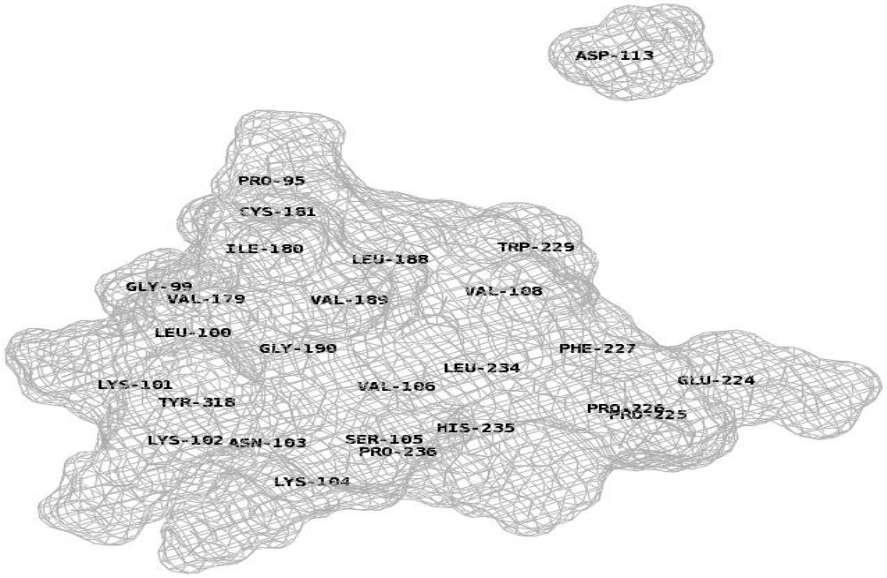

Figure 1: Pre-decided NNIBP.

2.6. Virtual screening and lead generation

Using TQ and a pyrazolo[1,5-a]pyridine-derived fragment as query pharmacophores, structurally similar compounds were assembled from public and commercial collections (SwissSimilarity/Swiss Institute of Bioinformatics resources, the PDB and ChEMBL ligand sets, and ZINC drug-like, lead-like and fragment-like subsets, plus the Aldrich CPR set). After fingerprint-, electroshape- and pharmacophore-based similarity filtering, an initial pool of ~1.6 × 10^7 compounds was reduced to ~7 000 candidates that were docked repeatedly against wild-type RT (2BAN) to obtain stable rankings. The two top-ranked, pocket-filling molecules were designated Ligand 1 and Ligand 2. A third compound (Ligand 3, the top virtual compound VC1 from a published CoMFA/CoMSIA 3D-QSAR study of 4-substituted pyridin-2-ones against wild-type and K103N/Y181C/Y188L RT) was carried forward as an independent, literature-anchored benchmark.

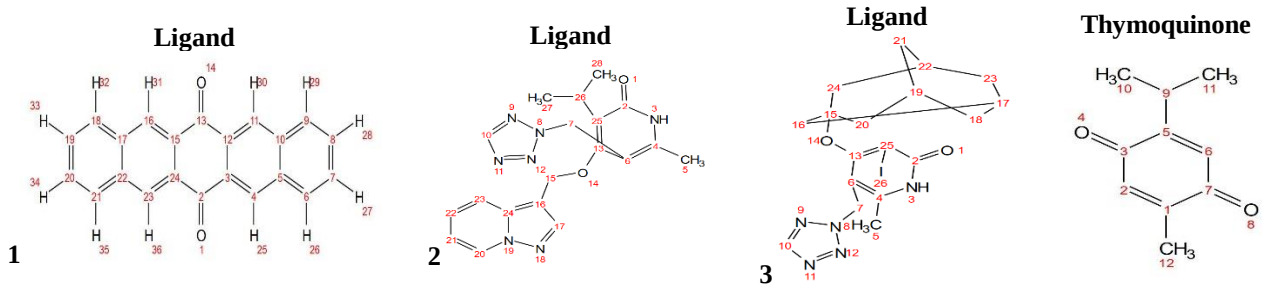

Figure 2: Molecular Structures of Selected Compounds.

2.7. In-silico ADMET and toxicity profiling

TQ, the three leads and efavirenz (reference NNRTI) were profiled in parallel on two independently maintained platforms. SwissADME provided physicochemical descriptors, Lipinski/Ghose/Veber/Egan/Muegge drug-likeness assessments, gastrointestinal-absorption and blood–brain-barrier estimates (BOILED-Egg), PAINS/Brenk structural alerts and synthetic-accessibility scores. ProTox-3.0 provided predicted oral LD50, toxicity class, and endpoint-specific probabilities, each accompanied by an applicability-domain confidence (average similarity

and prediction accuracy) that was used to decide whether a prediction could be interpreted.

3. RESULTS

3.1. Selection and mapping of resistance mutations

Table 1 summarises the three modelled substitutions and the single-mutant crystal structures used as templates. Each template contributes one experimentally determined mutant conformation, allowing the composite triple-mutant model to inherit locally accurate geometry at positions 103, 181 and 188 simultaneously.

Table 1: Resistance mutations incorporated into the composite HIV-1 RT model and the corresponding single-mutant crystal-structure templates.

Position / substitution	NNRTI relevance	Template (PDB)	Effect on inhibitor binding
Lys103 → Asn (K103N)	Class-defining; principal efavirenz/nevirapine mutation	3MED	Stabilises a closed pocket that impedes inhibitor entry
Tyr181 → Cys (Y181C)	Broad first-generation resistance	1JKH	Loss of aromatic π-stacking with the inhibitor
Tyr188 → Leu (Y188L)	Broad first-generation resistance	2YNF	Loss of key aromatic contact in the NNIBP

3.2. Homology model and stereochemical validation

The triple-mutant model (2BAP) was built from the ClustalW2 alignment of the edited target to the three single-mutant templates. Validation metrics are collected in Table 2. Relative to the wild-type parent, the initial 2BAP model showed a large improvement in Ramachandran core-region occupancy (75.2% → 96.0%) and in the ERRAT overall quality factor (65.25 → 78.86), indicating that comparative modelling produced a stereochemically superior structure rather than degrading the parent geometry. ProSA energy plots were consistent with a native-like fold across the sequence.

Table 2: Structure-quality metrics for wild-type RT (2BAN), the initial triple-mutant model (2BAP) and the model after 100 ns MD.

Structure	RMSD vs template (Å, MOE)	Ramachandran core (PROCHECK, %)	ERRAT overall quality factor
2BAN (wild-type)	—	75.2	65.25
2BAP (initial model)	1.871	96.0	78.86
2BAP (after 100 ns MD)	4.372	93.1	87.36

3.3. Molecular-dynamics equilibration of the model

The 100 ns simulation further improved packing quality: the ERRAT factor rose to 87.36 and Ramachandran core occupancy remained high at 93.1%, while the model-versus-template RMSD increased to 4.372 Å as the composite structure relaxed away from the idealised template geometry into a physically equilibrated conformation. Superimposition of the post-MD 2BAP structure on 2BAN confirmed conservation of the overall fold. The backbone RMSD-versus-time trace rose during the early trajectory and plateaued in the vicinity of 100 ns, indicating that the model had reached a stable basin suitable for use as a docking receptor.

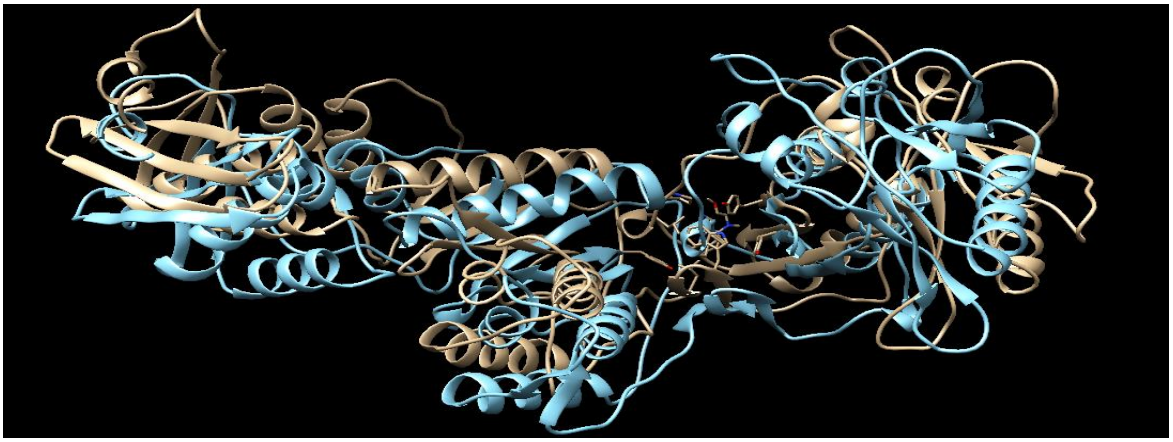

Figure 3: 2BAP (Model after Molecular Dynamics) superimposed on 2BAN. (Wild= Cyan)

3.4. Docking of thymoquinone across the RT panel

TQ was docked against wild-type and mutant RT in both blind and residue-restricted modes (Table 3). Under the pocket-restricted protocol, TQ bound with modest but consistent affinity across all five structures (−7.26 to −7.99 kcal mol⁻¹), and — notably — did not lose affinity at the resistance mutants; the strongest residue-based scores were obtained at Y188L (2YNF, −7.99) and at the triple mutant (2BAP, −7.89). This cross-mutant consistency established TQ as a viable seed pharmacophore, while its small size left the NNIBP incompletely filled — the structural argument for growing larger leads from it.

Table 3: Binding energies (kcal mol⁻¹) and representative hydrogen-bond contacts for thymoquinone across the RT panel.

Structure	Blind (kcal mol⁻¹)	Residue-based (kcal mol⁻¹)	Representative H-bond (blind)	Representative H-bond (residue-based)
2BAN (WT)	−6.87	−7.30	LEU26 (2.91 Å), ASN137 (2.69 Å)	THR139 (1.78 Å), GLY93 (1.79 Å)
3MED (K103N)	−6.44	−7.70	GLN182 (2.65 Å)	VAL90 (2.73 Å), THR139 (2.60 Å)
2YNF (Y188L)	−7.34	−7.99	THR165 (2.99 Å), PRO157 (2.85 Å)	LYS103 (2.83 Å), TYR318 (2.79 Å)
1JKH (Y181C)	−6.60	−7.26	SER162 (1.97 Å), ARG143 (2.20 Å)	ILE180 (2.66 Å), ARG172 (2.66 Å)
2BAP (triple)	−5.40	−7.89	THR470 (3.03 Å)	ILE382 (3.63 Å)

3.5. Virtual screening and lead identification

Similarity-guided assembly followed by iterative docking reduced an initial library of ~1.6×10^7 compounds to ~7 000 candidates and, ultimately, to two top-ranked leads against wild-type RT: Ligand 1 (6,13-dihydropentacene-6,13-dione, a planar pentacyclic quinone; Vina score −16.88 kcal mol⁻¹) and Ligand 2 (TQ-PZP-03, a pyrazolopyridine-substituted pyridin-2(1H)-one; −14.73 kcal mol⁻¹). Ligand 3 (VC1) was adopted from the literature 3D-QSAR study as an external benchmark. The pyridin-2(1H)-one scaffold of Ligands 2 and 3 is significant because it removes the reactive Michael-acceptor liability of the TQ quinone and installs the lactam N–H hydrogen-bond donor that anchors clinical pyridinone NNRTIs to Lys101 in the NNIBP.

leads occupied the NNIBP and made the pocket contacts predicted by the pyridinone pharmacophore. Second, and most important for the resistance problem, the binding scores were retained — rather than degraded — across the K103N, Y181C and Y188L mutants and against the composite triple mutant. Ligand 1 gave the strongest scores overall (residue-based −8.83 to −11.0 kcal mol⁻¹; −9.49 at the triple mutant), and the pyridinones held comparable, mutation-tolerant affinities (Ligand 3 residue-based −7.77 to −9.0; −8.28 at 2BAP). This is the pattern that first-generation NNRTIs conspicuously fail to show, where potency collapses at Y181C/Y188L. The flexible ether linker between the pyridinone and aryl portions is the design element intended to preserve binding as those residues mutate. We emphasise that these are docking scores and not measured affinities.

3.6. Docking of the leads across wild-type and mutant RT

The three leads were docked against the full panel in both modes (Table 4). Two features stand out. First, all

Table 4: Binding energies (kcal mol⁻¹) for the three leads across the RT panel, by docking mode (B = blind; R = residue-based).

Structure	Ligand 1 (B)	Ligand 1 (R)	Ligand 2 (R)	Ligand 3 (B)	Ligand 3 (R)
2BAN (WT)	−9.40	−8.83	−8.20	−7.00	−9.00
3MED (K103N)	−9.56	−7.60	−8.77	−7.77	−7.77
2YNF (Y188L)	−8.80	−8.80	−6.50	−6.84	−8.84
1JKH (Y181C)	−7.04	−11.0	−7.80	−7.00	−8.81
2BAP (triple)	−10.42	−9.49	−8.28	−8.28	−8.28

3.7. Molecular dynamics of the lead–enzyme complexes

Selected complexes were subjected to MD to test the persistence of the docked poses (Table 5). The wild-type complexes of TQ and Ligand 1, Ligand 2 and Ligand 3 equilibrated to low backbone RMSD values, consistent with stable occupancy of the pocket. Higher RMSD values indicate greater conformational adjustment and identify these pairings as priorities for longer-timescale simulation and free-energy analysis.

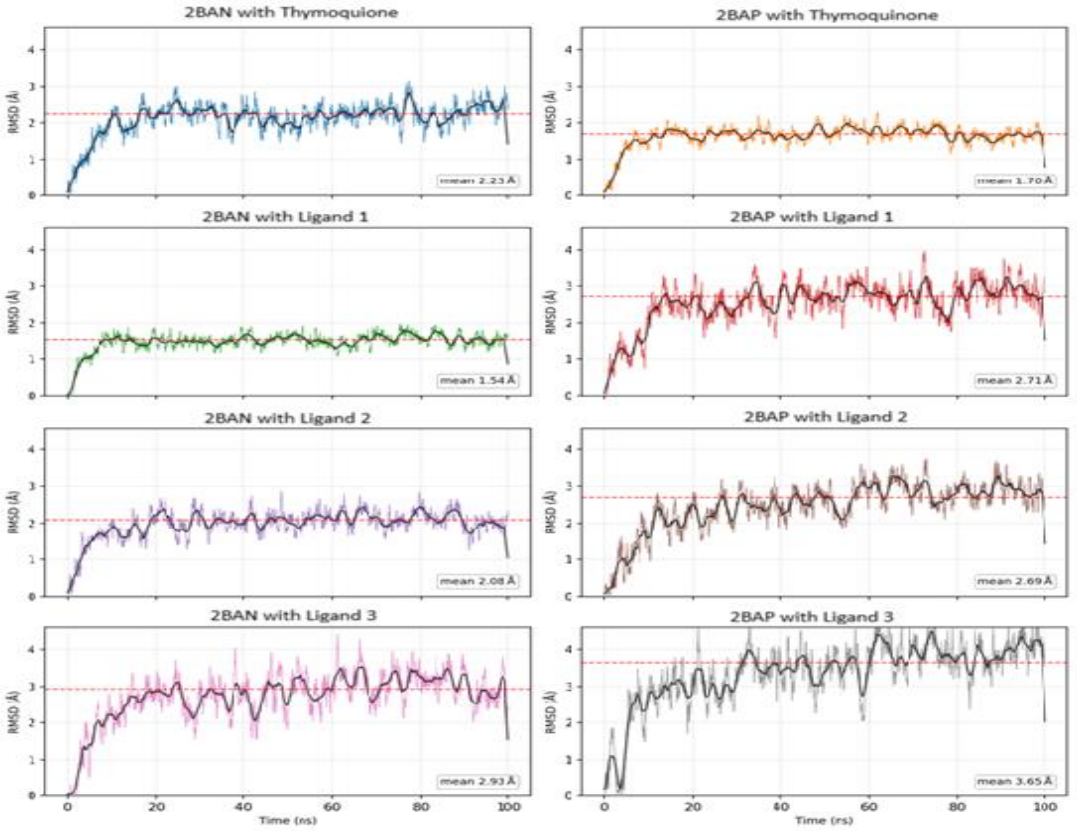

Figure 4: RMSD Comparison docked complexes.

3.8. In-silico ADMET and toxicity profiling

Physicochemical and drug-likeness descriptors are summarised in Table 6. TQ and both pyridinones passed the Lipinski, Ghose, Veber and Egan filters with high predicted gastrointestinal absorption. TQ triggered PAINS (quinone) and Brenk (Michael-acceptor) alerts — the very liabilities the scaffold hop is designed to remove — whereas the pyridinones carried no PAINS alerts. In ProTox profiling, the interpretability of each result was governed by applicability-domain confidence rather than the raw LD50. TQ returned a clean, high-confidence, non-mutagenic/non-hepatotoxic profile (100% similarity, 100% accuracy). Ligand 1, although high-confidence, carried the recognised liability signature of a planar polycyclic quinone (predicted mutagenicity 0.83; maximal mitochondrial-membrane-potential disruption; triple CYP inhibition) and was flagged for de-prioritisation. Critically, the efavirenz benchmark — a marketed NNRTI — itself returned only moderate similarity (60%), demonstrating that the low confidence scores of the designed pyridinones reflect sparse coverage of NNRTI chemical space, not intrinsic hazard; within its domain the model correctly reproduced efavirenz's documented CNS and hepatic toxicities. In-silico toxicity for the pyridinones is therefore reported as inconclusive, deferring to experimental genotoxicity/hepatotoxicity assays.

Table 5: Selected physicochemical, drug-likeness and predicted-toxicity descriptors (SwissADME; ProTox-3.0).

Descriptor	Thymoquinone	Ligand 1	Ligand 2	Ligand 3	Efavirenz
Formula	$C_{10}H_{12}O_2$	$C_{22}H_{12}O_2$	$C_{19}H_{21}N_7O_2$	$C_{18}H_{22}IN_5O_2$	$C_{14}H_9ClF_3NO_2$
MW (g mol^{-1})	164.20	308	379.42	467.31	315.67
Consensus Log P	1.94	4.78	2.61	2.99	4.07
GI absorption	High	High	High	High	High
Lipinski violations	0	0	0	0	0
PAINS alerts	1 (quinone)	1 (quinone)	0	0	0
ProTox LD50 (mg kg^{-1}) / class	2400 / 5	5000 / 5	4000 / 5	1000 / 4	600 / 4
ProTox domain confidence	High	High	Low (out)	Very low (out)	Moderate

4. DISCUSSION

The central methodological contribution of this work is a single, validated HIV-1 RT structure carrying the three dominant NNIBP resistance mutations at once. Evaluating candidates against single mutants in isolation is a weaker test than the clinic imposes, where multi-

mutant genotypes co-occur. Comparative modelling from three single-mutant crystal templates produced a composite model whose stereochemistry not only matched but exceeded that of the wild-type parent (Ramachandran 75.2% → 96.0%; ERRAT 65.25 → 78.86), and 100 ns of MD moved the structure into a physically equilibrated, high-quality state (ERRAT 87.36; RMSD plateau near 100 ns). The increase in template RMSD after MD is expected and desirable: it reflects relaxation away from idealised template geometry, not degradation, and is accompanied by improving packing statistics.

Against this receptor, the docking results converge on a single, resistance-relevant message. TQ is a small but genuine NNIBP binder whose affinity is retained across the mutant panel; its limitation is incomplete pocket filling and a reactive quinone, both of which the scaffold hop to a pyridin-2(1H)-one addresses. The derived pyridinone leads occupied the pocket as the established pharmacophore predicts and — unlike the first-generation NNRTIs whose clinical failure is defined by loss of potency at Y181C and Y188L — retained their docking scores across all four mutant contexts. The pentacenedione (Ligand 1) scored highest but is a planar polycyclic quinone with materials-science provenance and a corresponding toxicity signature, and is therefore de-prioritised despite its numbers. The pyridinones are the translationally sensible leads.

The ADMET analysis is as valuable for what it cannot resolve as for what it can. The efavirenz control demonstrates that the toxicity model's applicability domain does not adequately cover NNRTI chemical space, so the low confidence of the pyridinone predictions is a statement about the model, not the molecules. The correct inference is not that the leads are safe or unsafe, but that computation has reached its useful limit here and experimental toxicology is required.

Two limitations bound the interpretation. First, docking scores rank poses; they are not binding free energies, and the retained cross-mutant scores are hypotheses to be confirmed by rigorous free-energy methods (e.g., MM-GBSA/FEP) and by measured affinities. Second, the composite model, although well validated, is a model; convergence of the docking conclusions with the independent 3D-QSAR benchmark (Ligand 3) mitigates but does not eliminate model dependence. These considerations define the natural continuation of the work — the synthesis and enzymatic evaluation reported in the companion study.

5. CONCLUSIONS

We constructed and validated a triple-mutant (K103N/Y181C/Y188L) HIV-1 RT model that provides a clinically representative, resistance-focused platform for structure-based design, and used it to seed and prioritise thymoquinone-derived non-nucleoside leads. Model quality exceeded that of the wild-type parent and improved further under 100 ns of MD. Thymoquinone bound the NNIBP with mutation-tolerant, if modest, affinity, and rational scaffold-hopping to pyridin-2(1H)-one leads produced molecules that both filled the pocket and retained their docking scores across the resistance panel — the property that first-generation NNRTIs lack. In-silico ADMET supported the drug-likeness of the pyridinone leads while explicitly delimiting the reliability of toxicity prediction in this chemical space. Collectively, the validated model and the retained cross-mutant profiles constitute a testable, structure-based rationale for the experimental synthesis and enzymatic evaluation of the leads, which are reported in the companion paper.

Declaration of competing interest

The authors declare that they have no known competing financial interests or personal relationships that could have appeared to influence the work reported in this paper.

Data availability

Crystal structures are available from the RCSB PDB under accessions 2BAN, 3MED, 1JKH and 2YNF. The coordinates of the 2BAP model and docking input files are available from the corresponding author on reasonable request.

REFERENCES

1. UNAIDS. Global HIV & AIDS statistics — fact sheet 2025. Geneva: Joint United Nations Programme on HIV/AIDS, 2025.
2. International AIDS Society–USA. 2025 update of the drug resistance mutations in HIV-1. Top Antivir Med., 2025; 33(2): 457–67.
3. Ren J, Nichols CE, Chamberlain PP, et al. Mechanistic basis of NNRTI resistance for K103N and Y181C substitutions in HIV-1 reverse transcriptase. Viruses, 2016; 8(10): 263.
4. Xu HT, Asahchop EL, Oliveira M, et al. Molecular mechanism of antagonism between the Y181C and E138K mutations in HIV-1 reverse transcriptase. J Virol, 2011; 85(23): 11300–8.
5. Reddy N, Papathanasopoulos M, Steegen K, Basson AE. K103N, V106M and Y188L significantly reduce HIV-1 subtype C phenotypic susceptibility to doravirine. Viruses, 2024; 16(9): 1493.
6. Rhee SY, Gonzales MJ, Kantor R, et al. The Stanford HIV drug resistance database. Nucleic Acids Res., 2003; 31(1): 298–303.
7. Šali A, Blundell TL. Comparative protein modelling by satisfaction of spatial restraints. J Mol Biol., 1993; 234(3): 779–815.
8. Webb B, Šali A. Comparative protein structure modeling using MODELLER. Curr Protoc Bioinformatics, 2016; 54: 5.6.1–5.6.37.
9. Larkin MA, Blackshields G, Brown NP, et al. ClustalW and ClustalX version 2.0. Bioinformatics, 2007; 23(21): 2947–8.
10. Hall TA. BioEdit: a user-friendly biological

sequence alignment editor and analysis program. Nucleic Acids Symp Ser., 1999; 41: 95–8.
11. Guex N, Peitsch MC. SWISS-MODEL and the Swiss-PdbViewer: an environment for comparative protein modeling. Electrophoresis, 1997; 18(15): 2714–23.
12. Laskowski RA, MacArthur MW, Moss DS, Thornton JM. PROCHECK: a program to check the stereochemical quality of protein structures. J Appl Crystallogr, 1993; 26(2): 283–91.
13. Colovos C, Yeates TO. Verification of protein structures: patterns of nonbonded atomic interactions (ERRAT). Protein Sci., 1993; 2(9): 1511–19.
14. Wiederstein M, Sippl MJ. ProSA-web: interactive web service for the recognition of errors in three-dimensional structures of proteins. Nucleic Acids Res., 2007; 35: W407–10.
15. Phillips JC, Braun R, Wang W, et al. Scalable molecular dynamics with NAMD. J Comput Chem., 2005; 26(16): 1781–802.
16. Humphrey W, Dalke A, Schulten K. VMD: visual molecular dynamics. J Mol Graph., 1996; 14(1): 33–8.
17. Morris GM, Huey R, Lindstrom W, et al. AutoDock4 and AutoDockTools4: automated docking with selective receptor flexibility. J Comput Chem., 2009; 30(16): 2785–91.
18. Trott O, Olson AJ. AutoDock Vina: improving the speed and accuracy of docking with a new scoring function, efficient optimization, and multithreading. J Comput Chem., 2010; 31(2): 455–61.
19. O'Boyle NM, Banck M, James CA, et al. Open Babel: an open chemical toolbox. J Cheminform, 2011; 3: 33.
20. Irwin JJ, Shoichet BK. ZINC — a free database of commercially available compounds for virtual screening. J Chem Inf Model., 2005; 45(1): 177–82.
21. Daina A, Michielin O, Zoete V. SwissADME: a free web tool to evaluate pharmacokinetics, drug-likeness and medicinal chemistry friendliness of small molecules. Sci Rep., 2017; 7: 42717.
22. Banerjee P, Kemmler E, Dunkel M, Preissner R. ProTox 3.0: a webserver for the prediction of toxicity of chemicals. Nucleic Acids Res., 2024; 52: W513–20.
23. Lipinski CA, Lombardo F, Dominy BW, Feeney PJ. Experimental and computational approaches to estimate solubility and permeability in drug discovery and development settings. Adv Drug Deliv Rev., 2001; 46(1–3): 3–26.
24. Debnath U, Verma S, Jain S, et al. 3D-QSAR (CoMFA/CoMSIA) and protein-informatics analysis of 4-benzyl/benzoyl pyridin-2-ones as NNRTIs active against wild-type and mutant HIV-1 reverse transcriptase. (Reference 3D-QSAR study).
25. Zhou Z, Guo J, Li X, et al. Structure-based drug design yields diarylpyrimidine derivatives as potent HIV-1 NNRTIs. ACS Infect Dis., 2025; 11(9): 2607–16.